Journal of Power Sources 261 (2014) 285–291

Contents lists available at ScienceDirect

Journal of Power Sources

journal homepage: www.elsevier.com/locate/jpowsour

Long cycle life lithium ion battery with lithium nickel cobalt manganese oxide (NCM) cathode

Shuang Liu [a,*], L. Xiong [b], C. He [c]

[a] University of Electronic Science and Technology of China, Chengdu 610054, China
[b] Paramount Sciences, Cleveland, OH 44111, USA
[c] Chengdu Yanbai Technology Co. Ltd., Chengdu 610054, China

HIGHLIGHTS

- Characterized lithium ion batteries under extensive cycling (>3000 cycles).
- Achieved long cycle life (>3000 cycles) with $LiNi_{1-x-y}Co_xMn_yO_2$ cathode.
- Importance of cathode composition and electrode design for long cycle life.
- Possible capacity fade mechanisms were discussed.

ARTICLE INFO

Article history:
Received 17 December 2013
Received in revised form
21 February 2014
Accepted 19 March 2014
Available online 26 March 2014

Keywords:
Long cycle life
Lithium ion
Characterization
Lithium nickel cobalt manganese oxide
cathode

ABSTRACT

Lithium ion batteries with lithium nickel cobalt manganese oxide (NCM) cathode were characterized by extensive cycling (>2000 cycles), discharge rate test, hybrid pulse power characterization test (HPPC), and electrochemical impedance spectroscopy (EIS). The crystal structure, morphology and particle size of cathode materials were characterized by X-ray diffraction and scanning electron microscopy (SEM). It was demonstrated that the rate performance and cycle life of battery are closely related to the cathode material composition and electrode design. With proper selection of cathode composition and electrode design, the lithium ion battery cell achieved close to 3500 cycles with 85% capacity retention at 1C current.

1. Introduction

Lithium ion batteries have drawn a lot of attention as one of the most promising power sources for electric vehicles (EV) or hybrid electric vehicles (HEV), and residential energy storage applications [1–3]. Unfortunately, the high energy density and cycle life requirements for these applications necessitate further improvement of the present lithium ion batteries. Electrode materials play an important role in achieving these requirements, and considerable efforts have been devoted to develop new cathode materials and new structured materials [4,5].

Lithium nickel cobalt manganese oxides (NCM), $LiNi_{1-x-y}Co_xMn_yO_2$, are attractive alternative to $LiCoO_2$ as cathode materials for lithium ion batteries due to their relative low cost, high capacity, and better thermal stability [6–10]. The capacity and thermal stability of NCM strongly depend on composition, especially Ni content. Higher Ni content in NCM is responsible for higher reversible capacity because of the main redox species of Ni. However, high Ni content also leads to lower structural and thermal stabilities when NCM cathode is deeply charged, increasing the solid-electrolyte interfacial impedance. For instance, the $LiNi_{1/3}Mn_{1/3}Co_{1/3}O_2$ cathode has good thermal stability and delivers discharge capacities of 150–160 mAh g^{-1} when charged to 4.3 V. However, the capacity of $LiNi_{1/3}Mn_{1/3}Co_{1/3}O_2$ is not sufficient for PHEVs application [10]. On the other hand, Ni rich NCM, such as $LiNi_{0.8}Co_{0.1}Mn_{0.1}O_2$ have been intensively investigated as positive electrode materials for EV applications because of their relatively high reversible capacity, about 200 mAh g^{-1}. Unfortunately, they have shown poor thermal stability and poor cycle life. The thermal instability is due to oxygen release from the highly delithiated NCM, which reacts with the organic electrolyte and causes thermal runaway [11]. Meanwhile, the reduction of Ni^{4+} in the delithiated NCM to inactive NiO results in high solid-electrolyte interfacial

* Corresponding author. Tel.: +86 83208687; fax: +86 83206481.
E-mail address: shuangliu@uestc.edu.cn (S. Liu).

http://dx.doi.org/10.1016/j.jpowsour.2014.03.083
0378-7753/

impedance and poor cycle life of the cell [12]. The compromise between high capacity, cycle life, and thermal stability leads to the development of NCM in which the Ni content is between $LiNi_{0.8}Co_{0.1}Mn_{0.1}O_2$ and $LiNi_{1/3}Mn_{1/3}Co_{1/3}O_2$. It was reported that introduction of stable tetravalent Mn in the layered $LiNi_xCo_{1-2x}Mn_xO_2$ reduces the interfacial impedance, leading to a significant improvement of cell cycle life and thermal stability [8].

The relative high energy density, good thermal stability and cycle life of NCM have made it a promising candidate for commercial applications. However, the characterization of NCM cathodes was mainly investigated in coin cells, where typically less than a few hundreds of cycles were conducted [13–16]. For applications such as EV/PHEV and stationary power application, the evaluation of full cells with extended cycle life test is desired. For instance, 5000 charge-depleting cycles and 15 years of calendar life are required for the PHEV application with 40-mile electric drive battery [17]. We present here the characterization of pouch cells with NCM cathode and graphite anode under extensive cycling (>2000 cycles). The effects of cathode composition and electrode design on cycle life were investigated. The possible capacity degradation mechanism was also discussed.

2. Experimental

All experiments were performed on lithium ion battery pouch cells that were assembled with lithium nickel cobalt manganese oxides (NCM) as cathode, synthetic graphite as anode, polyethylene as separator, and 1.15 M LiPF6 in EC/EMC (1:3) as electrolyte. All electrode materials were purchased from commercial suppliers without modification. The cathodes consist of 92% active material, 4% conductive carbon black, and 4 wt% poly(vinylidene fluoride) (PVDF). The anodes consist of 85% active material, 8% conductive graphite, and 7% PVDF. The electrodes were obtained by mixing active materials, conductive additives, and PVDF in NMP, coating the slurry onto a current collect (Al for cathode, Cu for anode), drying the electrodes, and roll pressing to targeted thickness. The porosity of cathodes was kept constant (~30%). The electrodes were finally vacuum dried at 120 °C before cell assembly.

Electrochemical tests were conducted on Maccor testers. Five pouch cells were prepared for each test to ensure the reproducibility of the results. For discharge rate test, the pouch cells were charged at 0.5C rate to 4.2 V, kept at 4.2 V until current decreases to 0.05C (CC-CV protocol), and discharged at various C rates to 2.7 V. The cycling test was conducted at 1C current for both charge and discharge between 4.2 V and 3.0 V at 25 °C. The impedance change during cycles was monitored by electrochemical impedance spectroscopy (EIS), which was performed in the frequency range from 1 kHZ to 50 mHZ with ac amplitude of 10 mV. The pouch cells were also characterized by the application of the hybrid pulse power characterization (HPPC) test following the FreedomCAR battery test manual for plug-in hybrid vehicles [18].

XRD patterns were collected on a Phillips X-ray diffractometer with Cu Kα radiation. Data were collected between 15° and 90° at a scan rate of 0.01°/s. The lattice constants a and c and the fraction of transition-metal atoms (assumed to be Ni) in the lithium layer were determined using Rietveld refinements with Reitica software. The morphology and composition of the cathode powders were also examined by scanning electron microscopy (SEM, Hitachi S-900) and energy dispersive spectroscopy (EDS) attached to the SEM.

3. Results and discussion

Fig. 1 shows the XRD patterns and Rietveld fit of two commercial NCM materials that were employed as cathodes. The two NCM cathode powders has atomic ratio of Ni, Co, Mn close to 50:20:30 and 40:30:30, respectively, according to EDS analysis (Table 1), and therefore is referred to as NCM523 and NCM433, respectively for simplicity. The XRD patterns of NCMs in Fig. 1 can be well fitted by the α-$NaFeO_2$ structure with space group R-3m. The refined lattice constants and the fraction of transition-metal atoms in the lithium layer for the cathode samples were also listed in Table 1. For the refinements, it was supposed that Ni^{2+} ions located with the 3b site can be exchanged with Li^+ occupied at the 3a site due to similarity of their ionic radii (Li^+ = 0.76 Å, Ni^{2+} = 0.69 Å). The NCM433 exhibits lower degree of cation mixing and smaller lattice parameter compared to NCM523 (Table 1). The reduced degree of cation mixing is largely due to increased Co content, because Co^{3+} has

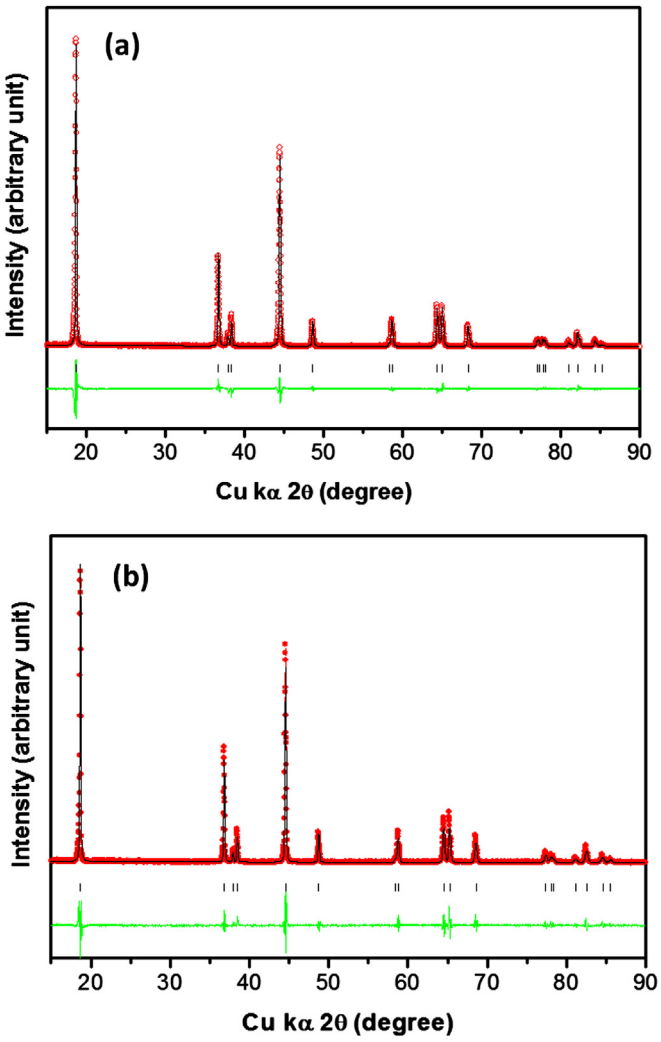

Fig. 1. XRD pattern and Rietveld refinement of cathode powers: (a) NCM523, (b) NCM433. Circles and lines correspond, respectively, to the observed and calculated intensities. The difference between the observed and calculated patterns and the peak positions corresponding to the O3 type phase are also shown.

Table 1
Crystal structural parameters and compositions of cathode powders.

Cathode	Crystal structural parameters from XRD				Composition from EDS		
	a (Å)	c (Å)	Volume (Å^3)	Cation mixing (%)	Ni (%)	Co (%)	Mn (%)
NCM 523	2.868	14.234	101.421	3.6	49.7	20.1	30.2
NCM 433	2.855	14.202	100.244	2.1	38.2	28.5	33.4

lower occupation in the Li layer due to the larger difference in radius between Co^{3+}(0.55 Å) and Li^{+}(0.76 Å). The increase of Co^{3+} and Mn^{4+} (0.53 Å) (Table 1) that have smaller radius than Ni^{2+} or Ni^{3+} (0.60 Å) also leads to smaller lattice parameter for NCM433 [10].

The morphology of the two cathode powders was also examined by scanning electron microscopy (SEM), as illustrated in Fig. 2. The particles in both samples are predominately spherical (Fig. 2(a) and (b)). The particle size distributions for both samples are summarized in Fig. 2(c) and (d). In both samples, the particle sizes are centered about 6–6.5 μm with standard deviation of 1.7–2.2 μm.

Pouch cells with NCM as cathode and graphite as anode were charged at 0.5C and discharged at various currents, and the representative discharge profiles are illustrated in Fig. 3(a)–(c). The average normalized capacity was also plotted against discharge current in Fig. 3(d), in which error bars are shown to represent the data distribution. The cell designs were based on the capacity data for anode and cathode in half cells (versus Li), and anodes were employed in excess to balance the irreversible loss of capacity due to the formation of the solid electrolyte interface (SEI) layer at the anodes, and to prevent lithium deposition at the end of charge. The cells with NCM523 and NCM433 share similar cell design except cathode composition (capacity ratio of negative electrode to positive electrode, or N/P ratio = 1.06). In addition, a group of cells were prepared with NCM433 but with lower cathode loading (same anode and therefore higher N/P ratio, N/P ratio = 1.19, referred to as NCM433′). The cell with NCM523 (Fig. 3(a)) shows slightly higher capacity than that with NCM433 (Fig. 3(b)). The higher capacity of the cell with NCM523 is mainly due to higher cathode specific capacity (162 mAh g^{-1} for NCM433 versus 167 mAh g^{-1} for NCM523 between 2.7 V and 4.3 V versus Li), because the capacity of NCM increases with Ni content [10]. However, compared to the cell with NCM523, the one with NCM433 shows less capacity decay when discharge current increases from 0.2C to 3C (Fig. 3(d)), which indicates that NCM433 has higher rate capability since NCM532 and NCM433 have similar particle size (Fig. 2). The higher rate capability of NCM433 is related to reduced cation mixing (Table 1), which impedes Li^{+} transport. The cell with higher N/P ratio (NCM433′) shows lower capacity (Fig. 3(c)) due to reduced cathode loading, but it also shows less capacity decay with increasing current (Fig. 3(c) and (d)) indicating better rate capability. The better rate performance of NCM433′ is mainly due to thinner cathode that has shorter diffusion path for Li ion intercalation/de-intercalation.

The area specific impedance (ASI) was measured at 4C discharge pulse current rate using HPPC procedure in accordance with the FreedomCAR battery test manual for PHEVs. Fig. 4(a) shows the typical cell voltage and current profile for the test. HPPC test consists of a series of pulse profile that contains pulse discharge (4C/10 s), rest step (40 s) and regenerative pulse charge (3C/10 s) followed by 1C-discharge for 10% of calculated capacity obtained from the formation cycles. The average area specific impedance (ASI) for 4C HPPC discharge as function of depth of discharge (DOD) is

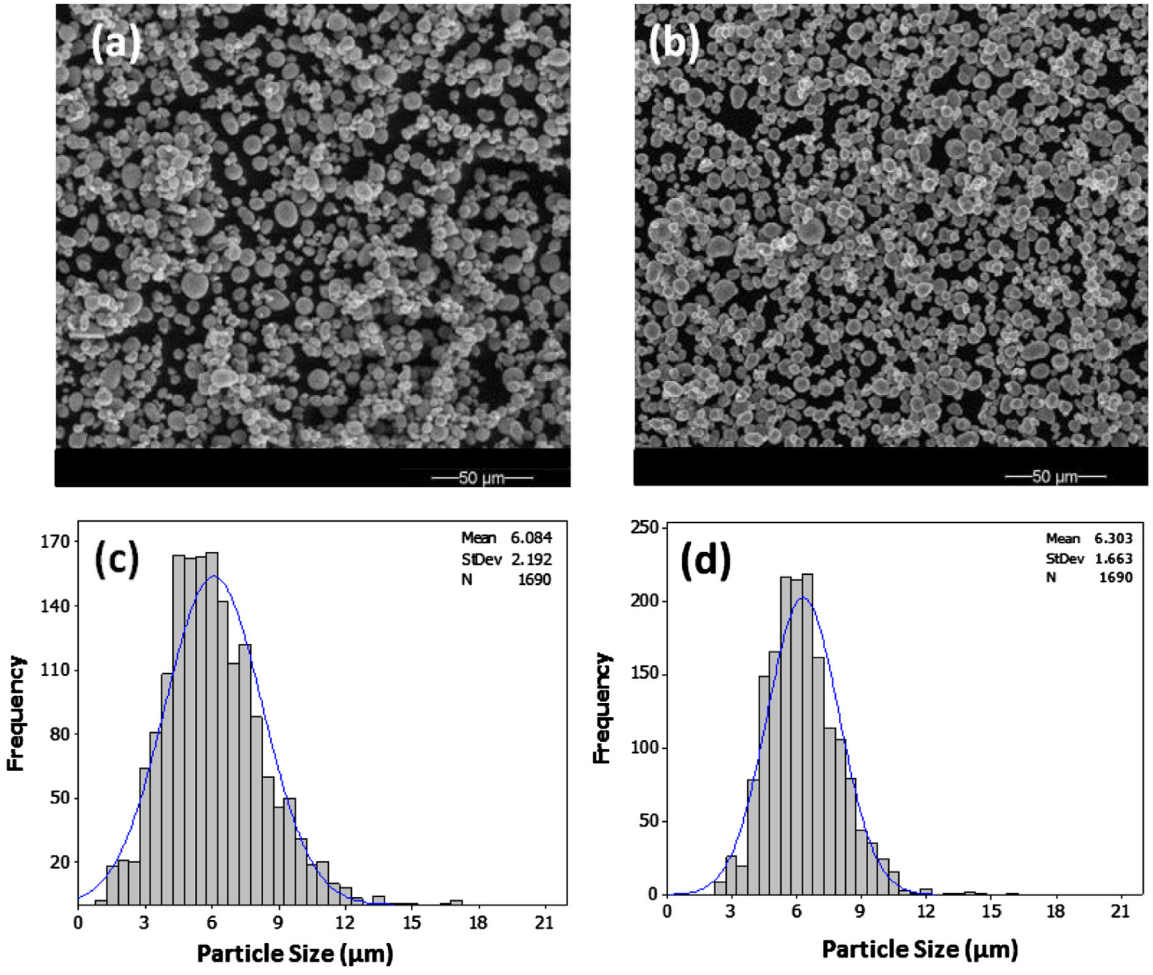

Fig. 2. SEM micrograph of cathode powders: (a) NCM523 and (b) NCM433. (c) and (d) is particle size distribution in (a) and (b), respectively.

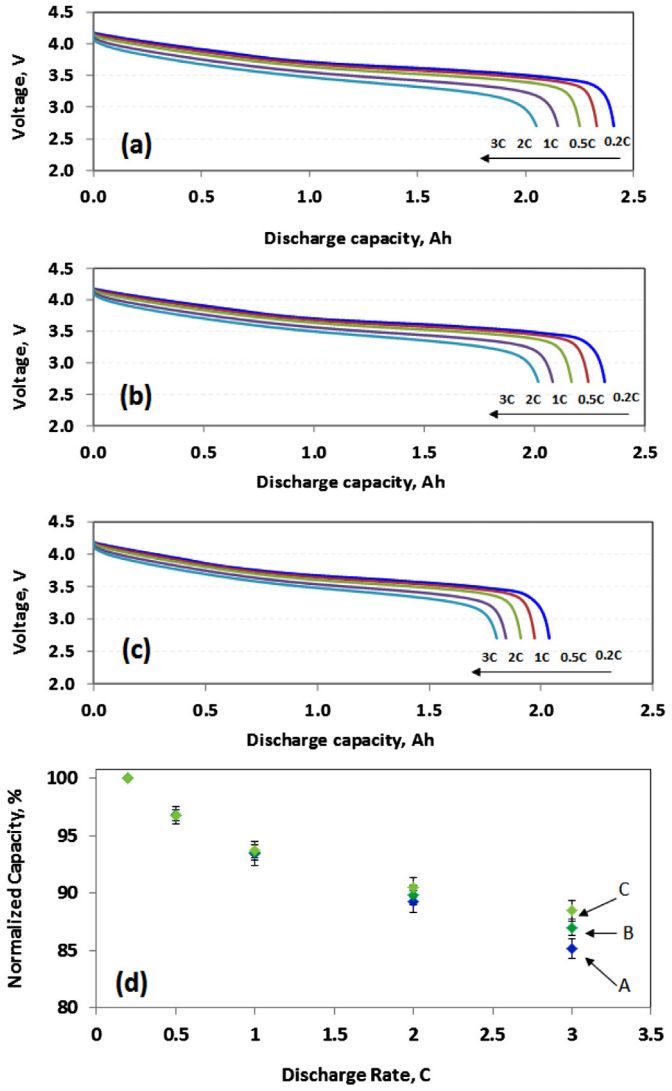

Fig. 3. Representative discharge profile of full cells with (a) NCM523, (b) NCM433, and (c) NCM433′ at various currents. (d) Normalized average discharge capacity at various C rates for NCM cathodes, A: NCM523, B: NCM433, C: NCM433′.

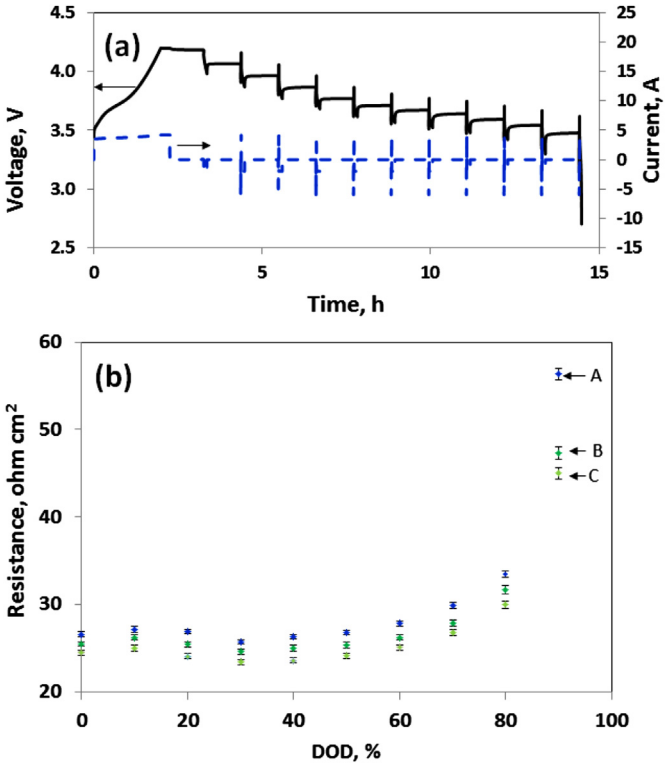

Fig. 4. (a) Representative HPPC test profile of a full cell with NCM523, (b) the resulting average ASI during discharge at various depth of discharge (DOD) for cells with A: NCM523, B: NCM433, C: NCM433′.

shown in Fig. 4(b). Compared to the cells with NCM523, those with NCM433 show lower ASI, and those with NCM433′ show the lowest ASI. It was also found that the cells with lower ASI also have higher rate performance (Fig. 3(d)). The ASI values obtained here are comparable to what were reported in the literature and meets or exceeds USABC-DOE requirement [7].

Long term cycling tests on pouch cells with NCM cathodes were carried out at 1C charge and 1C discharge current and the results are shown in Fig. 5. Each data point in the figures is the average of 5 cells. The cells with NCM523 show a little higher capacity at the beginning (Fig. 5(a)), but the capacity degrades faster than other cells. On the other hand, the cells with NCM433′ show slightly lower capacity than other two cells due to lower cathode loading but demonstrate the best cycling performance. The capacity retention (%) versus cycle for the three cells was plotted in Fig. 5(b). All three cells show excellent cycling performance with >2000 cycles at 80% capacity retention and the best cell (NCM433′) shows ~85% capacity retention after close to 3500 cycles. The good cycle life and relative high capacity of NCM make it a promising candidate for commercial applications such as EV/PHEV and stationary power application. More close comparison between the three types of cells is shown in Fig. 5(c), in which data points were selected from Fig. 5(b) up to 2300 cycles with error bars (<2%) to represent the overall distribution of the data. It is evident that the cells with NCM433 show better cycling performance than that with NCM523, which indicates that cathode composition plays an important role in cycle life. Meanwhile, cells with NCM433′ show the best cycling performance among all three cells, indicating electrode design also has important effects on cycle life. Past investigations on cycle life of NCM are mostly conducted on coin cells with a few hundreds of cycles. However, it was found in this study that it is hard to distinguish the performance difference between NCM cathodes with subtle difference in composition by limited cycles. For instance, the capacity retention at less than 500 cycles is almost indistinguishable between the three cells (Fig. 5(b)). In addition, for applications such as HEV, EV or stationary power application, where long cycle life is important, short term cycling is not enough to evaluate the durability of lithium ion batteries.

In order to understand the difference in cycle life among the three cells, the differential capacity dQ/dV was plotted against cell voltage over various cycles, shown in Fig. 6. Differential capacity measurements versus potential and cycle number offer greater sensitivity to probe cell degradation over a cycle life test [19]. Fig. 6(a) shows the differential capacity versus cell voltage at various cycle numbers up to 2000 cycles for the cell with NCM 523. As cycling proceeds, the dQ/dV peaks for Li^+ de-intercalation shift to higher voltages, while the dQ/dV peaks for Li^+ intercalation shift to lower voltages. In addition, the dQ/dV peak magnitude decreases with cycles. The decay of dQ/dV peak may indicate the loss of active materials [19]. The shift of dQ/dV peaks may resulted from the relative shift or slippage in capacity of the two electrodes in the cell caused by SEI growth and/or electrolyte oxidation [19], or increase of polarization caused by increase of internal resistance [20]. The

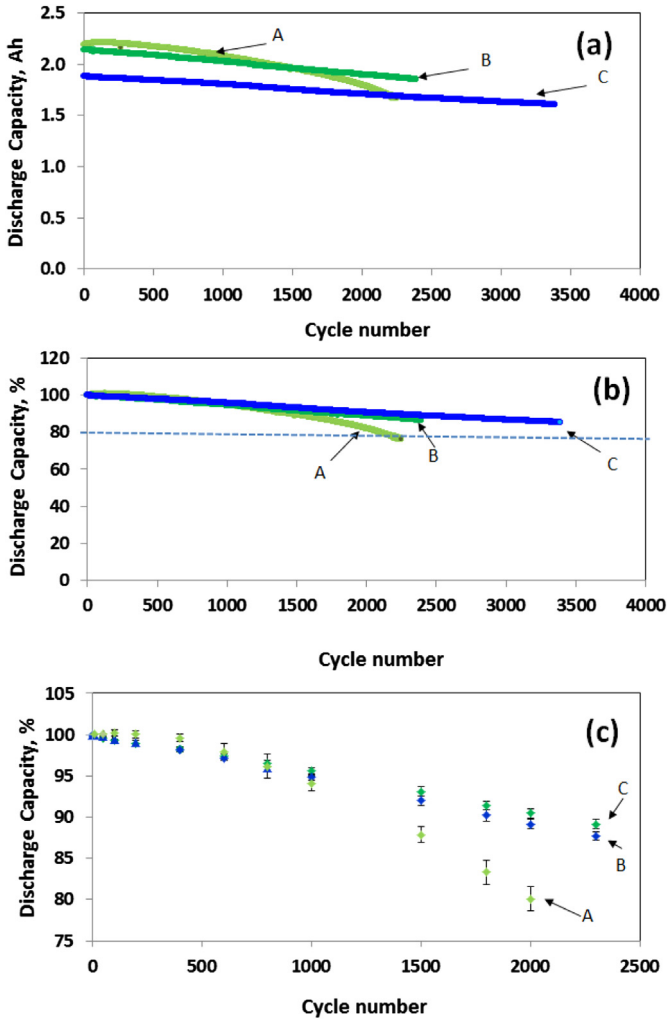

Fig. 5. Capacity (a) and capacity retention (b) as function of cycle number for full cells with A: NCM523, B: NCM433, C: NCM433′. (c): Data selected from (b) showing cycling performance up to 2300 cycles with error bars to represent data distribution. Cells were charged at 1C and discharged at 1C at room temperature.

cell with NCM433 cathode shows less dQ/dV peak decay and less dQ/dV peak shift (Fig. 6(b)) compared to that with NCM523 (Fig. 6(a)), which may result from cathode composition difference since both cells share similar cell design. On the other hand, the cell with NCM433′ shows the least dQ/dV peak decay and peak shift with cycles (Fig. 6(c)), indicating that electrode design also plays an important role.

Electrochemical impedance spectroscopy (EIS) was used to estimate the overall resistances of the cells during cycling. Fig. 7(a)–(c) shows the Nyquist plots of cells during 1st, 1000th, and 2000th cycle. The overall cell impedance is the sum of the positive and negative electrode impedances and the electrolyte resistance. Both anode and cathode impedances include contributions from solid electrolyte interface (SEI) at the surface of electrodes, the charge transfer resistance at the electrode–electrolyte interface. However, contribution from each of these resistances could be determined only by conducting EIS studies on individual electrodes. As shown in Fig. 7, the cell overall impedance increases with cycles indicated by the size increase of the semi-circles. However, the cell with NCM523 (Fig. 7(a)) shows more impedance increase than that with NCM433 (Fig. 7(b)). The cell with NCM433′ cathode shows the least impedance increase (Fig. 7(c)).

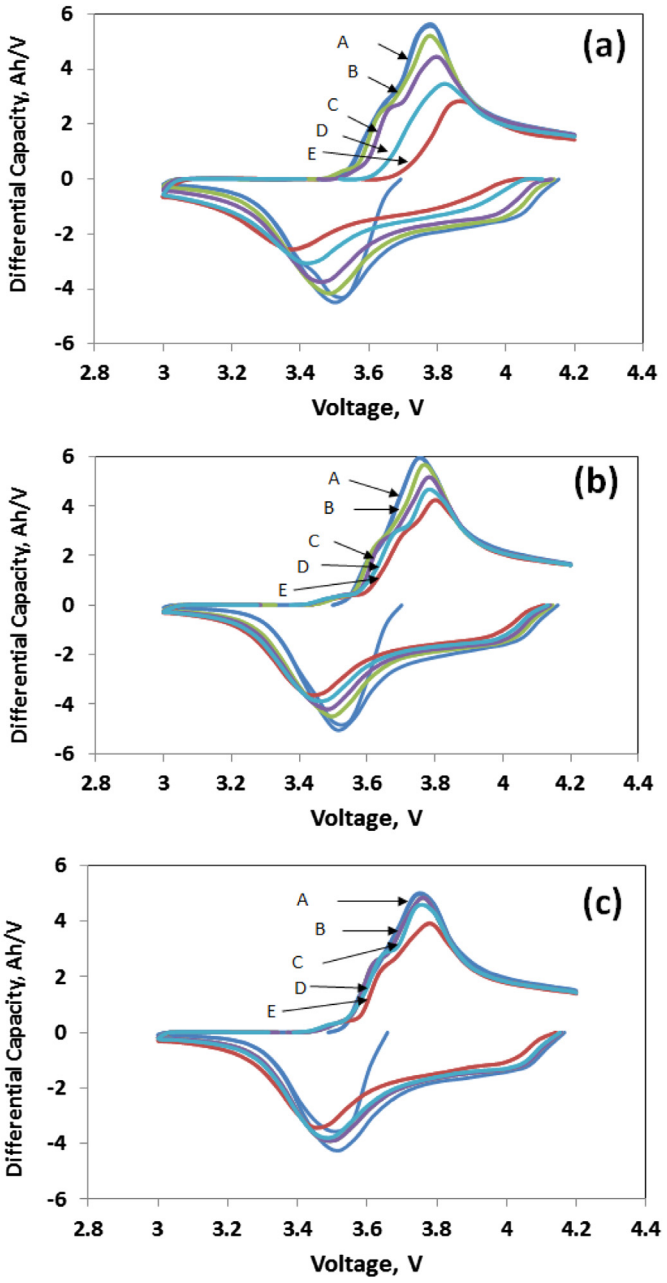

Fig. 6. Differential capacity as function of voltage for (a) NCM523, (b) NCM433, and (c) NCM433′ at various cycles after formation, A:1st cycle, B:300th cycle, C: 600th cycle, D: 1200th cycle, E: 2000th cycle.

From the correlation between cycling performance (Fig. 5) and EIS data (Fig. 7), it is evident that the impedance rise with cycles contributes to capacity fade. The rise in cell impedance may be due to formation and growth of SEI on anode [21], formation of inactive oxide on cathode surface that acts as obstacles to Li intercalation/deintercalation [22], dissolution of metal ions from cathode [23]. Compared to high temperature and/or high voltage (>4.3 V) cycling, the dissolution of metal ions in NCM at room temperature and normal voltage (4.2 V) is insignificant [24]. The cells with lower Ni content (NCM433) shows better cycling performance, mainly due to increased cathode structural and interfacial stability resulting from reduced cation mixing and decrease of unstable active species of Ni [10]. NCM with higher Ni content exhibits structural transformation near the surface region that increases the

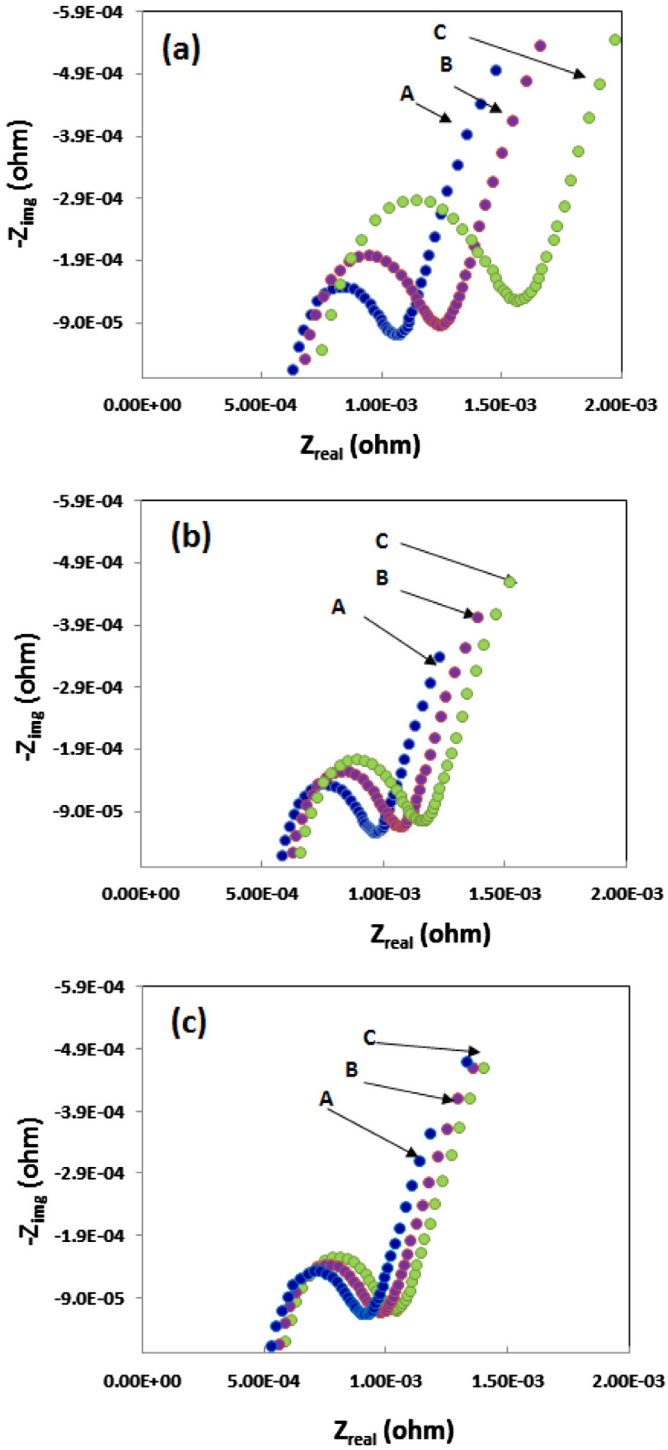

Fig. 7. Electrochemical impedance spectroscopy (EIS) of full cells with (a) NCM523, (b) NCM433, and (c) NCM433′ at various cycles after formation, A: 1st cycle, B: 1000th cycle, C: 2000th cycle.

charge-transfer resistance between the positive electrode and the electrolyte during electrochemical cycling [25]. In addition, the formation of inactive Ni (II) and Ni (IIII) which acts as obstacles to Li intercalation/deintercalation [22], also leads to cathode active material loss in electrode and contributes to capacity fade. The peak decay with cycle in the dQ/dV plot (Fig. 6) may indicate active material loss. Furthermore, the marginally higher Mn^{4+} content in NCM433 (Table 1) may also contribute to the improved cycle

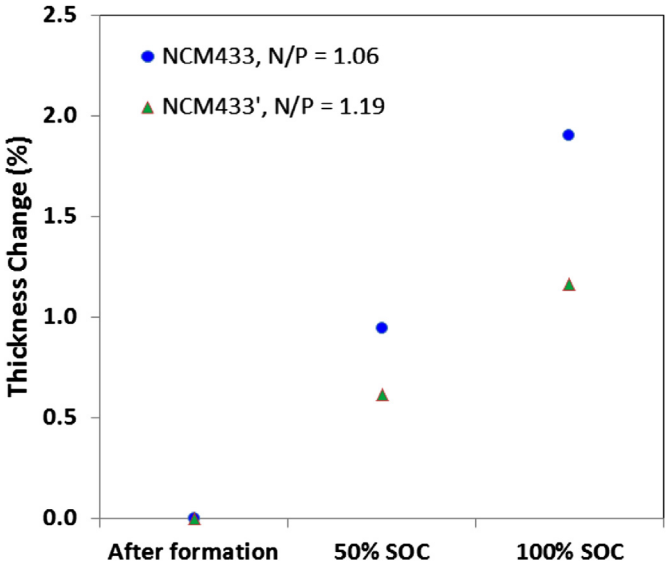

Fig. 8. Full cell thickness change (%) as function of state of charge (SOC) during formation with NCM 433 at different N/P ratios.

stability, as the cycling performance and thermal stability of NCM are sensitive to Mn^{4+} content [8].

The improved cycling performance of NCM433′ compared to NCM433 illustrates the importance of electrode design. Electrode thickness, electrode porosity, chemical composition and N/P ratio are among the important factors in electrode design [26,27]. NCM433′ cells share the same chemical composition and electrode porosity with NMC433 cells but are thinner in cathode (lower loading) and higher in N/P ratio. Thinner electrodes usually show lower internal resistance and better mechanical integrity, which in turn lead to better cycle life [26]. Results of N/P ratio study in a three electrode cell indicated that anode is charged to a lower state of charge (SOC) at higher N/P ratio (or more excess anode) [27], which results in less volume change or less strain during cycling. This is evident from the cell thickness change when the cells were charged to 0%, 50% and 100% SOC, shown in Fig. 8, where the cell with higher N/P ratio shows less thickness increase during charge. It was reported that cell thickness change is mainly contributed by graphite anode [28] and mechanical strain is one of the major degradation mechanisms for graphite anode [29]. Further study is ongoing to further understand the effect of electrode design on cycling performance.

4. Conclusions

Lithium ion batteries using NCM cathode and graphite anode have demonstrated long cycle life (>3000 cycles). It was found that cathode material composition, electrode design have important effects on rate performance and cycle life. Compared to the cells with NCM523, those with NCM433 shows higher rate performance, less impedance rise during cycling and better cycle life, which may be due to more stable cathode structure with less Ni content and less cation mixing. Cells with thinner cathode and slightly higher electrode N/P ratio also shows improved rate performance and cycle life, due to lower cell impedance and less cell volume change during cycling.

Acknowledgments

This work was supported by the National Natural Science Foundation of China (Grant No. 61177035), Sichuan Provincial

International Cooperation Project (2013HH0002) and Sichuan Provincial Science and Technology Support Project (2011GZ0003, 12ZC0245, 2012GZ0051). The authors would also like to thank CCD Research Center of China Electronics.

References

[1] A.S. Arico, P. Bruce, B. Scrosati, J.-M. Tarascon, W.V. Schalkwijk, Nat. Mater. 4 (2005) 366–377.
[2] T.T. Kojimaa, T. Ishizua, T. Horibaa, M. Yoshikawab, J. Power Sources 189 (2009) 859–863.
[3] K. Darcovicha, E.R. Henquina, B. Kenneya, I.J. Davidsona, N. Saldanhab, I. Beausoleil-Morrison, Appl. Energy 111 (2013) 853–861.
[4] B.L. Ellis, K.T. Lee, L.F. Nazar, Chem. Mater. 22 (2010) 691–714.
[5] Y. Wang, G. Cao, Adv. Mater. 20 (2008) 2251–2269.
[6] I. Belharouak, W. Lu, D. Vissers, K. Amine, Electrochem. Commun. 8 (2006) 329–335.
[7] B.-R. Lee, H.-J. Noh, S.-T. Myung, K. Amine, Y.-K. Sun, J. Electrochem. Soc. 158 (2011) A180–A186.
[8] Y.-K. Sun, H.-B. Kang, S.-T. Myung, J. Prakash, J. Electrochem. Soc. 157 (2010) A1335–A1340.
[9] Z. Li, N.A. Chernova, M. Roppolo, S. Upreti, C. Petersburg, F.M. Alamgir, M.S. Whittingham, J. Electrochem. Soc. 158 (2011) A516–A522.
[10] K.-S. Lee, S.-T. Myung, K. Amine, H. Yashiro, Y.-K. Sun, J. Electrochem. Soc. 154 (2007) A971–A977.
[11] J. Cho, H. Jung, Y. Park, G. Kim, H.S. Lim, J. Electrochem. Soc. 147 (2000) 15–20.
[12] D.P. Abraham, R.D. Twesten, M. Balasubramanian, I. Petrov, J. McBreen, K. Amine, Electrochem. Commun. 4 (2002) 620–625.
[13] F. Zhou, X. Zhao, J.R. Dahn, J. Electrochem. Soc. 156 (2009) A343–A347.
[14] I. Belharouak, Y.-K. Sunb, J. Liua, K. Amine, J. Power Sources 123 (2003) 247–252.
[15] D. Li, C. Yuan, J. Dong, Z. Peng, Y. Zhou, J. Solid State Electrochem. 12 (2008) 323–327.
[16] J.D. Wilcox, E.E. Rodriguez, M.M. Doeffa, J. Electrochem. Soc. 156 (2009) A1011–A1018.
[17] U.S. Council for Automotive Research LLC, USCAR, http://www.uscar.org, (accessed 03.09.10).
[18] Idaho National Laboratory, Battery Test Manual for Plug-In Hybrid Electric Vehicles, http: // www.inl.gov/technicalpublications/Documents/4655291.pdf, (accessed 10.10.12).
[19] A.J. Smith, J.R. Dahn, J. Electrochem. Soc. 1 (2012) A290–A293.
[20] B.-C. Park, H.-B. Kim, S.-T. Myung, K. Amine, I. Belharouak, S.-M. Lee, Y.-K. Sun, J. Power Sources 178 (2008) 826–831.
[21] Y.-B. He, Z.-Y. Tang, Q.-S. Song, H. Xie, Y.–G. Liu, Q. Xua, J. Electrochem. Soc. 155 (2008) A481–A487.
[22] T. Sasaki, T. Nonaka, H. Oka, Chikaaki Okuda, Y. Itou, Y. Kondo, Y. Takeuchi, Y. Ukyo, K. Tatsumi, S. Mutob, J. Electrochem. Soc. 156 (2009) A289–A293.
[23] K. Amine, Z. Chen, Z. Zhang, J. Liu, W. Lu, Y. Qin, J. Lu, L. Curtis, Y.-K. Sun, J. Mater. Chem. 21 (2011) 17754–17759.
[24] H. Zheng, Q. Sun, G. Liu, X. Song, V.S. Battaglia, J. Power Sources 207 (2012) 134–140.
[25] S.-U. Woo, B.-C. Park, C.S. Yoon, J. Prakash, Y.-K. Sun, J. Electrochem. Soc. 154 (2007) A649–A655.
[26] H. Zheng, J. Li, X. Song, G. Liu, V.S. Battaglia, Electrochim. Acta 71 (2012) 258–265.
[27] S.S. Zhang, K. Xu, T.R. Jow, J. Power Sources 160 (2006) 1349–1354.
[28] J.H. Lee, H.M. Lee, S. Ahn, J. Power Sources 119–121 (2003) 833–837.
[29] V. Agubra, J. Fergus, Materials 6 (2013) 1310–1325.